STEM CELLS TRANSLATIONAL MEDICINE®

TISSUE-SPECIFIC PROGENITOR AND STEM CELLS

Very Late Antigen-5 Facilitates Stromal Progenitor Cell Differentiation Into Myofibroblast

NAMITA SEN,[a] MARK WEINGARTEN,[a] YAKOV PETER[a,b]

Key Words. Anchorage-independent cells • Stromal progenitor cells • Mesenchymal stromal cells • Myofibroblast development • Cell transplantation • Very late antigen-5

[a]Department of Biology, Yeshiva University, New York, New York, USA; [b]Department of Pulmonary Medicine, Albert Einstein College of Medicine, Yeshiva University, Bronx, New York, USA

Correspondence: Yakov Peter, Ph.D., Department of Biology, Yeshiva University, Belfer Hall No. 1406A, 500 West 185th Street, New York, New York 10033, USA. Telephone: 212-960-5401; E-Mail: peter@yu.edu

Received January 23, 2014; accepted for publication August 22, 2014; first published online in SCTM *Express* October 1, 2014.

1066-5099/2014/$20.00/0

http://dx.doi.org/10.5966/sctm.2014-0014

ABSTRACT

Fibrotic disease is associated with abrogated stromal cell proliferation and activity. The precise identity of the cells that drive fibrosis remains obscure, in part because of a lack of information on their lineage development. To investigate the role of an early stromal progenitor cell (SPC) on the fibrotic process, we selected for, and monitored the stages of, fibroblast development from a previously reported free-floating anchorage-independent cell (AIC) progenitor population. Our findings demonstrate that organotypic pulmonary, cardiac, and renal fibroblast commitment follows a two-step process of attachment and remodeling in culture. Cell differentiation was confirmed by the inability of SPCs to revert to the free-floating state and functional mesenchymal stem/stromal cell (MSC) differentiation into osteoblast, adipocyte, chondrocyte, and fibroblastic lineages. The myofibroblastic phenotype was reflected by actin stress-fiber formation, α-smooth muscle production, and a greater than threefold increase in proliferative activity compared with that of the progenitors. SPC-derived pulmonary myofibroblasts demonstrated a more than 300-fold increase in fibronectin-1 (*Fn1*), collagen, type 1, α1, integrin α-5 (*Itga5*), and integrin β-1 (*Itgb1*) transcript levels. Very late antigen-5 (ITGA5/ITGB1) protein cluster formations were also prevalent on the differentiated cells. Normalized SPC-derived myofibroblast expression patterns reflected those of primary cultured lung myofibroblasts. Intratracheal implantation of pulmonary AICs into recipient mouse lungs resulted in donor cell FN1 production and evidence of epithelial derivation. SPC derivation into stromal tissue in vitro and in vivo and the observation that MSC and fibroblast lineages share a common ancestor could potentially lead to personalized antifibrotic therapies. STEM CELLS TRANSLATIONAL MEDICINE *2014;3:1342–1353*

INTRODUCTION

Stem/progenitor cells are triggered to undergo proliferation and multipotential differentiation after tissue injury. The microenvironment imposes physical restrictions and conveys biochemical cues to regulate these processes. Identification of the physiological conditions and molecular signals that influence stem cells would help elaborate the differentiation programs activated during tissue regeneration.

Mesenchymal stem/stromal cells (MSCs) and fibroblasts are cells of major biological and medicinal importance. Although considered to be related through the stromal cell lineage, controversies remain regarding the definitive molecular and therapeutic properties of these cell types [1]. MSCs are known to moderate the inflammatory response after organ injury and to play an active role in tissue repair [2–4]. Fibroblast cells function in the deposition of extracellular matrix (ECM) networks, including collagen and fibronectin, supporting the over- and underlying (epithelial and endothelial) tissues. Activated fibroblasts, or myofibroblasts, are noted for their ability to trigger organ fibrosis, a process that results in the excessive and persistent formation of scar tissue. However, the developmental stage of the fibrotic cell and the contribution of other (nonfibroblastic) cells to their lineage differentiation remain unclear [5, 6].

Integrin protein heterodimers, consisting of one α (ITGA) and one β (ITGB) subunit, are a principal component involved in cell-cell and cell-ECM interactions and in the inward and outward transmission of signals across the cell membrane [5]. A number of integrins were used to identify hematopoietic, lung, neural, and additional progenitor cell types, including ITGA5, ITGA6, ITGB1, and ITGB4 [7–9]. Functionally, integrins enhanced human embryonic stem and fibroblast cell attachment and retained human embryonic stem cells in the pluripotential state on collagen, fibronectin, and laminin substrates [10–13]. Similarly, integrin ITGA5/ITGB1 (very late antigen-5 [VLA5]) heterodimers were reported to mediate hematopoietic progenitor cell attachment to bone marrow stroma. In contrast, ITGA6/ITGB1 (VLA6) expression was found to increase cell clearance from the lung [14]. However, because integrin expression patterns were shown to change with the cellular microenvironment, definitive links between

the properties and the activity of the progenitor cells and integrin biosynthesis and dimerization remain equivocal [15].

Using a method designed to model tissue regeneration ex vivo, we described an organotypic lung population of anchorage-independent cells (AICs) that proliferated and differentiated in suspension culture [16]. This physiologically distinct AIC population, which could be isolated from multiple organisms, including humans, was immunophenotypically mixed and included lung epithelial progenitor and hematopoietic subsets decorated by CD45, c-KIT, and/or the CD11b (ITGAM) integrin. The AICs were clonogenic and spontaneously developed into multicellular epithelial-like sheets and tissue-like spheres in culture. We hypothesized that this population additionally harbors stromal progenitor cells (SPCs). Stromal cells within the AIC population would provide structural and paracrine support for differentiating epithelium, which together would form a robust multicellular network of compensatory growth. In the present study, we investigated the existence of lung SPCs and monitored the molecular and cellular changes that coincide with their derivation into functional MSC and myofibroblastic lineages. We then validated myofibroblast differentiation from SPCs and elaborated on the retention and fate of mixed pulmonary AIC allografts in the lungs of immunocompetent mice.

Materials and Methods

Mice and Tissue Sources

Male and female mice, aged 1–2 months (C57BL/6), were purchased from Charles River Laboratories (Wilmington, MA, http://www.criver.com), and green fluorescent protein (GFP) and β-galactosidase-expressing mice were purchased from Jackson Laboratory (catalog nos. 003115 and 002073, respectively; Bar Harbor, ME, http://www.jax.org). All experiments were conducted in compliance with Institutional Animal Care and Use Committee protocols of Yeshiva University.

Cell Culture, Renewal, and Propagation Experiments

Tissue culture media and supplements, including Dulbecco's modified Eagle's medium (DMEM), bovine growth serum (BGS) or fetal bovine serum (FBS), and 1% penicillin-streptomycin were purchased from Life Technologies (Grand Island, NY, http://www.lifetechnologies.com) or Atlanta Biologicals (Lawrenceville, GA, http://www.atlantabio.com). Organotypic isolation of lung AICs has been previously described by our laboratory [16]. In brief, lung, heart, and kidney organs were extracted and minced into $\sim$1 mm^2 cubes with two randomly collected fragments submerged in a DMEM + 10% BGS (upper layer) situated on a polymerized (DMEM + 20% BGS) 3.3% alginate substrate (bottom layer). All cells were incubated at 37°C in a 5% CO_2 incubator.

Adhesion and Fibroblast Differentiation Experiments

AICs at day 7 were passaged onto coverslips or 12-well plastic dishes (Fisher Scientific International, Hampton, NH, http://www.fisherscientific.com). For the adhesion experiments, the coverslips or wells were soaked in 70% ethanol for 15 minutes, warmed to 37°C, and coated with 100 μl of 2% gelatin, 1 mg/ml fibronectin, or 50 μg/ml laminin. Excessive coat was aspirated, and the coverslips were allowed to dry for an additional 30 minutes to 1 hour. Single-suspended AIC clusters were collected and passaged onto these matrices. For the SPC experiments, the adhering cells cultivated in DMEM + 10% FBS were collected at day 7. For the fibroblast studies, SPCs (day 7) were dissociated in 0.025% trypsin/EDTA (Life Technologies), washed, and transferred onto fresh plates for proliferation. Passaged (P3-P7) myofibroblast cells were used for analysis. Cell counts were performed on a hemocytometer by two independent individuals on each passage.

Primary Culture of Mouse Lung Fibroblasts

Mouse lung tissue was minced in phosphate-buffered saline (PBS) and digested in collagenase/dispase for 1 hour at 37°C in a water bath with occasional shaking. The cells were filtered through a 40-μm filter into a 50-ml centrifuge tube and centrifuged for 10 minutes at 2,000 rpm at 4°C. Harvested cells were cultured on 100-mm tissue culture plates and incubated in 5% CO_2 at 37°C in DMEM + 10% FBS. The media were changed every 3–4 days and the cells collected for experimentation between P3 and P5.

Immunofluorescence

The cells were rinsed in cold PBS, fixed in 1% paraformaldehyde, and stained with selected primary reagents. These included goat anti-mouse fatty acid binding protein-4 (FABP4; 1:100), osteopontin (1:100) (both R&D Systems Inc., Minneapolis, MN, http://www.rndsystems.com), rabbit anti-phosphorylated-histone-3 (1:100; Sigma-Aldrich, St. Louis, MO, http://www.sigmaaldrich.com), epidermal growth factor receptor (1:100; Millipore, Billerica, MA, http://www.millipore.com), integrin α5 (ITGA5; 1:100; Cell Signaling Technology, Danvers, MA, http://www.cellsignal.com), integrin β1 (1:250; Abcam, Cambridge, MA, http://www.abcam.com), and mouse anti-prosurfactant protein C (1:1,000; Chemicon, Temecula, CA, http://www.chemicon.com), platelet growth factor receptor β (1:100; Santa Cruz Biotechnology Inc., Santa Cruz, CA, http://www.scbt.com), α smooth muscle actin type 1 (ACTA1; 1:100), β-actin (ACTB; 1:100), cellular fibronectin (1:100), and type 1 collagen (α1 and α2 heteromer; 1:100; Sigma-Aldrich). Rabbit anti-ITGA5 (Cell Signaling Technology) and anti-ITGB1 (Abcam) were also used. The cells were then washed and treated with either goat anti-mouse Alexa Fluor 488, chicken anti-goat Alexa Fluor 488 (1:500; Molecular Probes, Eugene, OR, http://probes.invitrogen.com), goat anti-rabbit cyanine-3 (1:500; Jackson ImmunoResearch Laboratories, Inc., West Grove, PA, http://www.jacksonimmuno.com) secondary antibodies or phalloidin-conjugated Alexa Fluor 488 (1:200; Life Technologies), and 4′6-diamidino-2-phenylindole (DAPI; Sigma-Aldrich). The tissue was covered with Fluoromount-G (SouthernBiotech, Birmingham, AL, http://www.southernbiotech.com).

Immunoblot Analysis

The cells were rinsed in cold PBS, solubilized in a boiling SDS sample buffer (8% SDS, 0.2 M Tris-HCl, pH 6.8, 10 mM EDTA, 40% glycerol) supplemented with protease inhibitors (protease inhibitor cocktail; Sigma-Aldrich), sheared through a 20-gauge syringe needle, and spun at 13,000*g* for 30 minutes. Western blots were performed as previously reported [17]. In brief, protein concentrations were determined (DC Protein Assay, Bio-Rad Hercules, CA, http://www.bio-rad.com), and 70 μg of protein was loaded and electrophoresed in 10% SDS-polyacrylamide gels (Pierce, Rockford, IL, http://www.piercenet.com), transferred onto

polyvinylidene fluoride membranes (Millipore), and incubated in the presence of primary antibodies at 4°C overnight. The primary antibodies included anti-ITGA5 (1:500), anti-ACTB (1:1,000), and anti-ACTA1 (1:1,000). Goat anti-mouse IRDye 800 CW or donkey anti-rabbit IRDye 680 secondary antibodies (1:10,000; LI-COR Biotechnology, Lincoln, NE, http://www.licor.com) were used. Protein detection was performed on an Odyssey IR scanner (LI-COR Biotechnology). For protein densitometry, the image background was subtracted from the measured (mean) band signal intensity using the ImageJ software package (NIH, Bethesda, MD, http://www.imagej.nih.gov/ij/). Standardized values (to that of the mean ACTB band intensity) were then taken for statistical analysis.

Flow Cytometry

The cells were washed and labeled per the manufacturer's instructions. The following antibodies were used: phycoerythrin (PE) conjugated rat anti-mouse ITGA6/CD49f (eBioscience Inc., San Diego, CA, http://www.ebioscience.com), PE conjugated rat anti-mouse ITGA5/CD49e (BD Pharmingen, San Diego, CA, http://www.bdbiosciences.com), PE conjugated hamster anti-mouse ITGB1/CD29 (Life Technologies), fluorescein isothiocyanate (FITC) conjugated rat anti-mouse integrin β-4 (Abcam), and mouse anti-BRDU (eBioscience) followed by goat anti-mouse Alexa Fluor 488 (Life Technologies). For the percentage of ACTA1 expression, a permeabilization step using the saponin-based permeabilization and wash reagent (Life Technologies) was added. The isotype controls included FITC conjugated rat-IgG, PE conjugated-rat and conjugated-hamster IgG, and Alexa Fluor 488-conjugated goat-IgG (SouthernBiotech). The cells were analyzed using an easyCyte mini-flow cytometer (Guava Technologies, Millipore), FACScan (Becton, Dickinson and Company, Franklin Lakes, NJ, http://www.bd.com), or a MoFlo3 (Dako, Fort Collins, CO, http://www.dako.com).

Nucleic Acid Purification, Reverse Transcription, Polymerase Chain Reaction, and Quantitative Polymerase Chain Reaction

RNA was isolated by the Trizol method (Invitrogen, Carlsbad, CA, http://www.invitrogen.com) and purified using RNeasy columns (Qiagen, Valencia, CA, http://www.qiagen.com). RNA quality and quantity were determined using NanoDrop spectrophotometry (Thermo Scientific, Wilmington, DE, http://www.nanodrop.com). First-strand cDNA synthesis using the SuperScript III reverse transcriptase kit (Life Technologies) was performed on 5 μg of total RNA using oligo(dT)12–18 (Life Technologies). All reactions were performed in an ABI-PRISM 7300 sequence detection system (Applied Biosystems, Life Technologies) starting with 10 minutes of *Taq* activation at 95°C, followed by 40 cycles of melting (95°C, 30 seconds), primer annealing (60°C–62°C, 30 seconds), extension (72°C, 30 seconds), and culminating with a melting curve analysis to validate polymerase chain reaction (PCR) product specificity. The absence of primer-dimers was verified after amplification using melting curve analysis. The quantitative PCR (qPCR) primer sequences used in the present study have been previously reported and are listed in supplemental online Table 1 [18]. For identification of Y-chromosomal sequences in female recipient mice, transplanted lungs were homogenized in DNA isolation buffer (50 mM Tris, pH 8.0, 0.5% SDS, 0.1 M EDTA), extracted in phenol/chloroform, and precipitated with ethanol. The PCR conditions included 30 cycles of 1 minute at 94°C, 30 seconds at 60°C, and 30 seconds at 72°C. The murine Y-linked sex determining region of chromosome Y (*Sry*) and X-linked methyl CpG binding protein 2 (*Mecp2*)-specific PCR primer sequences are listed in supplemental online Table 1.

MSC Functional Assays

These studies were performed using the mouse mesenchymal stem cell functional identification kit (R&D Systems; catalog no. SC010). In brief, SPC growth medium was replaced at day 7 with adipogenic induction medium (α-minimum essential medium supplemented with 10% FBS), and the cells were cultivated for an additional 10 days according to the manufacturer's protocol. Cell phenotype was assessed using Oil Red O, a lipid-specific stain, qPCR, and immunofluorescence. Osteogenic differentiation was induced by SPC culture in osteoinductive medium (+ 10% FBS) for 14 days. The cell phenotype was then assessed using alizarin red staining, which labels calcium-rich deposits, qPCR, and immunofluorescence. For chondrogenic differentiation, the SPCs were dissociated, washed, and transferred to chondrogenic induction culture media and incubated in 15-ml conical tubes per the manufacturer's instructions. The cultures were maintained for 2 weeks in chondrogenic medium before analysis, which included a trichrome stain that labels collagen and qPCR. The media were changed every other day.

AIC Processing, Transplantation, and Identification in Recipient Lungs

The AIC populations were cultivated for 2 weeks in vitro, washed, counted, and resuspended in PBS. Cell transplantation was performed by tracheal incision, as previously reported [19]. In brief, the mice were anesthetized with ketamine (75 mg/kg) and xylazine (5 mg/kg) i.p. at doses sufficient to allow spontaneous breathing yet provide surgical-concentration anesthesia. A small incision ($<$1 cm) was made parallel to the trachea, a tie was inserted beneath the trachea for positioning, and 50 μl of dissociated cells (1×10^6) in vehicle or in 0.013% trypsin were injected. The tie was removed and the wound closed with a single suture. After a 10–60-day period, the mice were sacrificed, and the lungs were harvested simultaneously, ensuring an even presentation of the experimental and control tissues. For the β-galactosidase experiments, the lungs were inflated and fixed (2% formaldehyde, 0.01% glutaraldehyde, 1:5,000 Nonidet-P40 in PBS, pH 7.2), stained in β-galactosidase solution (0.21% ferrocyanide, 0.16% ferricyanide, 0.0025% $MgCl_2$, 0.001% Nonidet-P40) with 1 mg/ml X-gal (Invitrogen), postfixed (0.5 M sodium phosphate, 0.0675 M sodium hydroxide, 4% formaldehyde, and 25% glutaraldehyde titrated to pH 7.2), processed further, embedded in paraffin, and sectioned. For the GFP transplantation studies, the lungs were inflated with Tissue-Tek (Sakura Finetek, Torrance, CA, http://www.sakura.com), frozen, cryostat-sectioned (Leica CM-3050S, Leica Biosystems, Nussloch, Germany, http://www.leicabiosystems.com) and stored at $-$80°C. The slides were then labeled using mouse anti-GFP (MAB3580; Millipore) followed by goat anti-mouse Alexa Fluor 488 (Molecular Probes). The background was subtracted, and the GFP signal intensity of murine lung sections was quantified using the Scion Image software application package, version 4.0.3.2 (Scion Corporation, Frederick, MD, http://www.scioncorp.com).

Photographic Capturing and Statistical Analysis

The images were serially captured under identical exposures using a motorized Olympus I81 fluorescent inverted microscope connected to a XM10 cooled CCD camera head using the cellSens dimension imaging software package (Olympus, Center Valley, PA, http://www.olympusamerica.com). Confocal microscopy was performed in the Analytical Imaging Core Facility at the Albert Einstein College of Medicine using a Leica AOBS SP2 confocal microscope (Leica Microsystems, Inc., Buffalo Grove, IL, http://www.leica-microsystems.com). Unless indicated otherwise, statistical analysis was performed using the *F* test for normally distributed data and the nonparametric Wilcoxon rank sum test for skewed data. Data are presented as the average ± SEM.

RESULTS

Cell Attachment to the Stratum Initiates an Irreversible Differentiation Program

A previous study of ours demonstrated the proliferation and differentiation of lung-isolated cells in suspension. These cells spontaneously form an epithelial-like sheet when attached to an alginate matrix. To test the ability of this population to generate stromal/mesenchymal cell types, we investigated the effect of a stiff substrate on cell growth. Passaging of AICs into the (suspension) media of a tissue culture plate resulted in maintenance of an anchorage-independent population and the attachment of select cells, henceforth referred to as stromal progenitor cells (SPCs) (Fig. 1A). AIC attachment occurred in 100% of the wells ($n > 500$). The SPCs were viable on the dish, which was demonstrated by trypan blue exclusion and annexin V and 7-aminoactinomycin D cytometry (data not shown). To clarify whether SPCs represent a more determined (AIC) cell type, we designed a series of experiments to test the subsequent generation of SPCs from AICs (Fig. 1B, path A) and, comparatively, the reverse transition of SPCs into AICs (Fig. 1B, path B). Cell growth and derivation were then quantified. First, passage (P) of free-floating AICs into the media phase of plastic (and glass) substrates resulted in the attachment of SPCs as early as 30 minutes after passage. To investigate whether cell attachment was dependent on protein synthesis, we repeated these experiments in the presence of Geneticin (500 μg/ml; Life Technologies), proven to block de novo protein production. Geneticin treatment did not affect cell attachment, implying that gene expression is not required for cell attachment. To test for selective cell affinity to ECM, we repeated these experiments on fibronectin-, laminin-, and gelatin-treated plates and found no differences in the percentage or time of cell attachment (data not shown). Subsequent passage of the free-floating cell population (Fig. 1B, path A) resulted in a reduced capacity of P2 cells to attach to the substratum (0.96% ± 0.1% of the cells), indicating that the colonizing cell subset was depleted from P1 floating cells. Finally, separated from the initial free-floating cell population (Fig. 1B, path B), the SPCs did not form a new free-floating AIC subset (data not shown). Taken together, these data indicate that a specified subset within the free-floating lung AIC population attaches to a stiff matrix in the absence of de novo gene expression and that cell transition to an anchoring phenotype is a unidirectional process that emulates canonical stem cell differentiation.

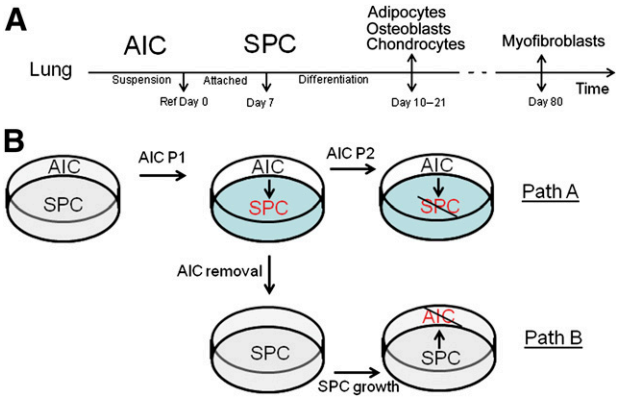

Figure 1. Experimental model of canonical stromal cell differentiation from free-floating lung populations. **(A):** Flowchart depicting the developmental timeline of stromal cell derivation from AICs. AICs were prepared as previously reported and cultivated for 7 days, indicated on the chart as "Ref Day 0." On this day, a clone of AICs was taken for lineage classification or passaged to generate the transient SPCs. SPCs were cultivated for an additional 7 days, at which point, they were differentiated toward mesenchymal or fibroblastic lineages. Adipocytes, osteoblasts, and chondrocytes were cultivated in differentiation media and characterized at days 10–21 and (myo) fibroblasts grown and characterized at day 80 in culture. **(B):** Flowchart depicting experiments performed to test the reversibility of stromal cell differentiation on attachment to a substrate. Path A depicts the attachment of P1 free-floating subsets and their maturation into SPCs. Additional passages (P2) resulted in diminished SPC differentiation. Path B illustrates the isolation of SPCs and their inability to revert to the more primitive free-floating population, establishing unidirectional stromal differentiation. Abbreviations: AIC, anchorage-independent cell; P, passage; SPC, stromal progenitor cell.

Proliferation and Functional SPC Differentiation Into MSC Lineages

AIC passage (P1) to a stiff substrate resulted in 6.4% ± 2.3% of the initial cell population attaching to the dish after 1 day in culture. By day 3 in vitro, the proportion of anchoring cells had significantly increased to 14.4% ± 4.9% ($n \geq 15$; $p = .002$) of the culture, with no observed change in the number of free-floating cells. Furthermore, because removal of AICs from the coculture did not deter attached cell growth, these data suggest that the increased number of anchoring cells results from adhering cell proliferation and not the delayed attachment of free-floating cells. Accordingly, although P1 AICs did not progress toward a proliferative cell phenotype in suspension, 9.7% ± 3.1% of the attached SPC clones (1,000–2,000 cells; $n \geq 20$) developed proliferative fibroblast-like properties with time in culture ($n = 10$; $p = .01$).

Next, to examine the differentiation potential of day-7 SPCs (Fig. 1A), we attempted to differentiate these cells into adipocyte, osteoblast, and chondrocyte lineages using functional MSC assays. SPCs cultivated in adipocyte derivation media for a period of 10 days displayed adipocyte phenotypes, manifested by peroxisome proliferator-activated receptor γ (*Pparg*) production, which stimulates lipid uptake and adipogenesis in fat cells, FABP4 expression, and the presence of lipid deposits in the differentiated cells, shown by Oil Red O staining (Fig. 2). In turn, the cultivation of SPCs in osteoblast-conditioned media for 14 days resulted in increased osteopontin gene and protein expression, and alizarin red staining, which detects the presence of calcium deposits, an early marker of matrix mineralization. Finally, SPCs could develop into cells of the chondrocyte lineage as early as 17 days in culture, which was

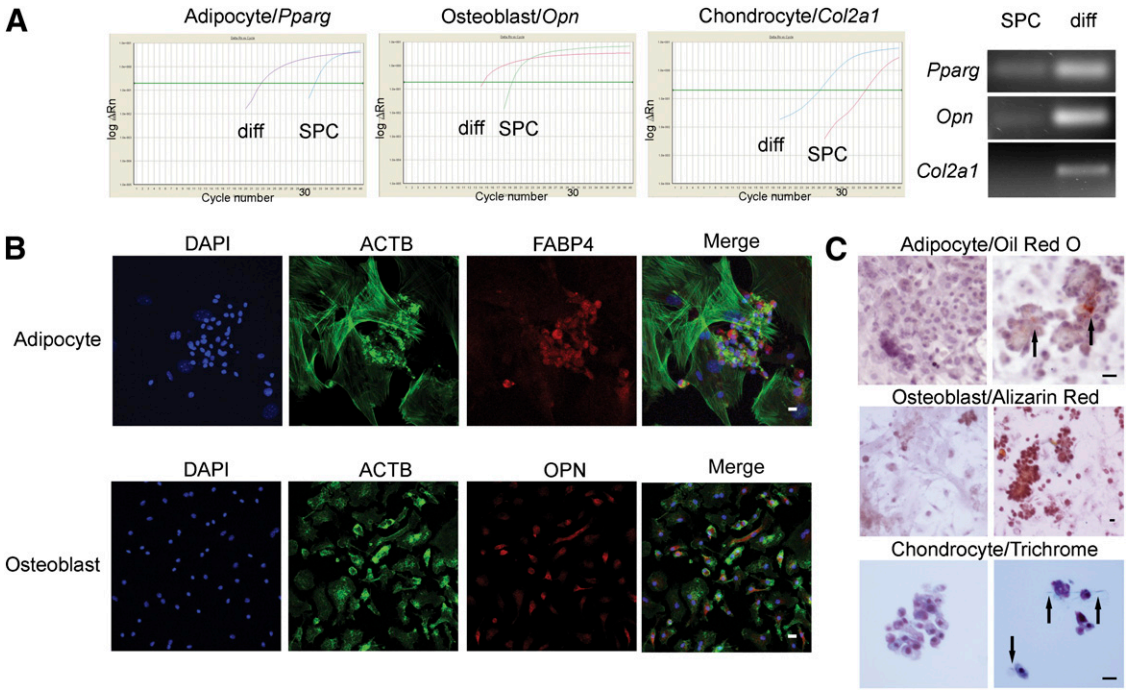

Figure 2. Stromal progenitor cells possess functional properties of mesenchymal stem/stromal cells (MSCs). Day 7 SPCs were conditioned in MSC differentiation media for 10–21 days and the lineages determined by quantitative polymerase chain reaction (PCR) and cytochemistry. **(A):** Left: Representative amplification plots of SPC and differentiated cells depict earlier amplification (cycle number) of *Pparg*, *Opn*, and *Col2a1* in differentiated adipocytes, osteoblasts, and chondrocytes, respectively. Right: PCR amplicons from a separate batch of SPCs and differentiated adipocytes (*Pparg*), osteoblasts (*Opn*), and chondrocytes (*Col2a1*). These results indicate higher amounts of gene transcript expression (cDNA template) in differentiated cell types. **(B):** Immunofluorescence of differentiated SPCs. SPCs were cultured in MSC differentiation media and prepared for immunofluorescence. Above: Differentiated adipocytes were labeled for (from left to right): DAPI nuclear stain (blue), phalloidin-Alexa Fluor 488, which binds to the actin cytoskeleton (ACTB; green), FABP4 (red), and Merge. Below: Differentiated osteoblasts were labeled for (from left to right) DAPI nuclear stain (blue), ACTB (green), OPN (red), and Merge. **(C):** Immunocytochemistry of differentiated SPCs. Cultivated in growth (control; left) or cell-differentiation media (right), slides were stained with Oil Red O (adipocyte), which labels lipids and fatty acids red, alizarin red, which stains calcium-rich deposits (osteoblast), or trichrome stain, which interacts with collagen to produce a blue hue (chondrocytes). Arrows in adipocyte and chondrocyte panels demonstrate regions of dense cellular staining. Scale bars = 20 μm. Abbreviations: ACTB, β-actin; *Col2a1,* collagen type 2 α1; DAPI, 4′6-diamidino-2-phenylindole; diff, differentiation; FABP4, fatty acid binding protein-4; *Opn,* osteopontin; *Pparg,* peroxisome proliferator-activated receptor γ; SPC, stromal progenitor cell.

determined by collagen type 2 α1 transcript and collagen protein production, established by qPCR and trichrome immunochemistry, respectively. Collagen synthesis is an important function of cartilaginous cells. Although adipocyte, osteoblast, and chondrocyte differentiation might be physiologically irrelevant in lung tissue, these data suggest that the SPC population can serve as a source of lung MSCs.

Mature Stromal Cells Demonstrate Greater Proliferation Rates Than Their Progenitors

Involved in numerous disease processes, the most abundant mesenchymal cell type of the lung is considered to be the fibroblast. Therefore, to determine the ability of SPCs to generate fibroblasts, we continued cell cultivation in common growth media, instead of switching to differentiation media. Under these conditions, SPCs grew slowly until increasing proliferative activity at day 14 to comprise $65 \pm 25 \times 10^3$ cells (P3) at day 21 (Fig. 3A). At day 80, a staggering $34 \pm 6 \times 10^6$ cells (P7) were found, with the cells maintaining the properties of proliferative growth. We then sought to confirm DNA synthesis in SPCs by measuring incorporation of the thymidine analog bromodeoxyuridine (BrdU) into cell nuclei. At day 7, 1.4% $\pm$ 0.3% of the SPC subset displayed BrdU labeling; at day 80 (cells displaying fibroblast morphology), the proportion had increased to 3.6% $\pm$ 1.1% cells (Fig. 3B, 3C; $n \geq 4$). This increase was statistically significant ($p = .01$), which, in contrast to convention, indicates a mature cell that proliferates faster than its progenitor. The mitotic activity of SPCs and fibroblast-like cells could be further validated by nuclear localization of phophsporylated-histone-3 (Fig. 3D–3G and 3H–3K, respectively). These changes were accompanied by a spherical transition to a flattened morphological phenotype, elevated fibronectin-1 (FN1), ACTA1 expression, and actin stress fiber formation. Together, these factors reflect myofibroblastic cell development (supplemental online Fig. 1). The increase in ACTA1 production was statistically significant, as seen by densitometric analysis of immunoblot assays ($p < .01$; $n = 3$), with a representative immunoblot shown in supplemental online Figure 2. Elevated protein levels of collagen type 1 α1 (COL1A1) complemented the observed increases in FN1 and ACTA1 expression (data not shown). Importantly, fibroblast growth factor 1 treatment expedited early spherical epidermal growth factor receptor expressing cell remodeling into a flattened and elongated platelet-derived growth factor receptor β-1-positive lineage after 2 weeks in culture (supplemental online Fig. 3). These findings suggest that SPCs, through proliferative growth, cell remodeling, and ECM protein expression, develop, in long-term cultures, a phenotype that emulates cultured myofibroblasts.

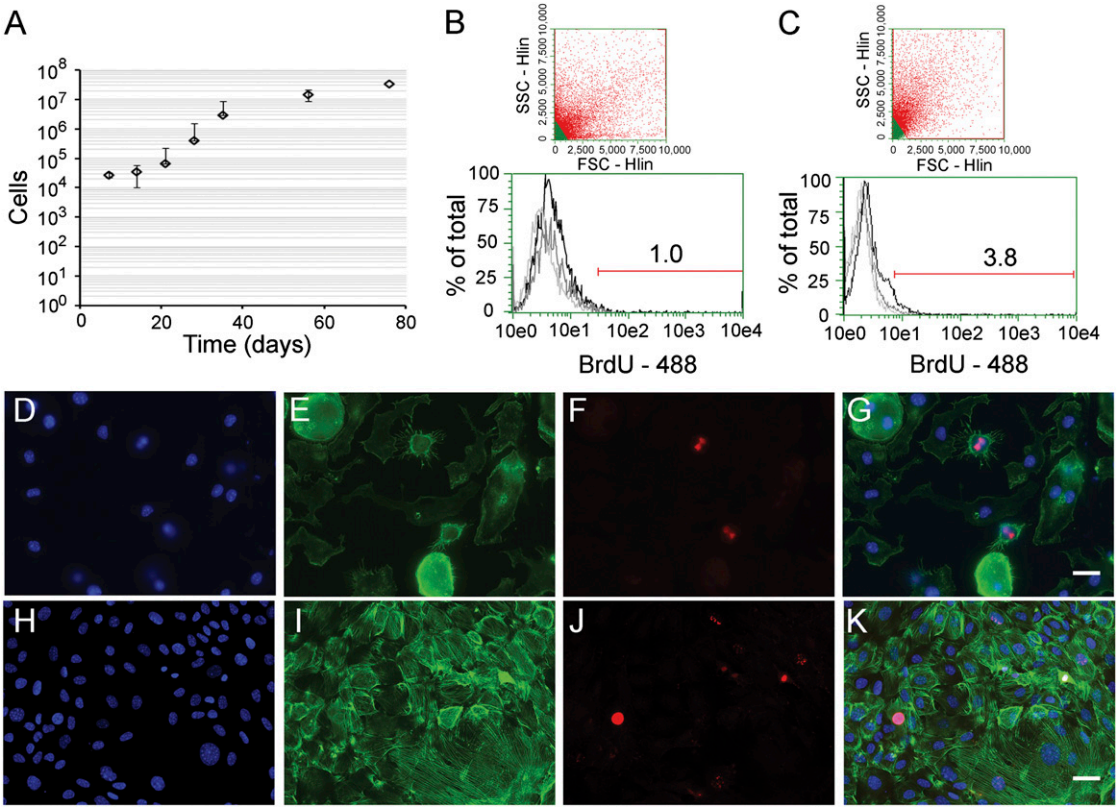

Figure 3. Stromal lineage proliferation increases with cell differentiation. Passaged stromal progenitor cells were cultivated and counted or tested for cell cycling activity with time in culture. **(A):** Growth curve illustrating increased stromal cell numbers with time in culture. **(B):** Representative flow cytometry dot plot depicting gating of the stromal progenitor population (day 7; above) and a histogram showing the percentage of BrdU-positive cells in the total population (below). **(C):** Representative flow cytometry dot plot depicting gating of SPC-derived myofibroblasts (day 80; above) and the proportion of the population incorporating BrdU (below). Black, BrdU treated; gray, isotype controls; light gray, untreated control cells. Representative micrographs of cells labeled for phosphorylated-histone 3, a common marker for DNA replication. **(D–G):** SPCs labeled for DAPI nuclear stain (**[D]**; blue), the actin binding drug phalloidin (**[E]**; green), phosphorylated-histone 3 (**[F]**; red), and Merge **(G)**. **(H–K):** SPC-derived myofibroblasts (day 80) stained for DAPI nuclear stain (**[H]**; blue), actin (**[I]**; green), phosphorylated-histone 3 (**[J]**; red), and merge **(K)**. Scale bars = 20 μm. Abbreviations: 488, Alexa Fluor 488; BrdU, bromodeoxyuridine; DAPI, 4′,6-diamidino-2-phenylindole; SPC, stromal progenitor cell.

Changes in Transcript Expression Accompany Cell Differentiation Into a Fibroblastic Lineage

To identify the molecular changes associated with fibroblast differentiation, we investigated the expression of epithelial, endothelial, and myofibroblastic lineage markers and compared the changes in their relative levels to the baseline AICs (P1; reference, day 0). Although *Acta1* expression in day-7 SPCs did not significantly change, the *Fn1*, *Col1a1*, and CCAAT/enhancer-binding protein α (*Cebpa*; $n \geq 4$; Table 1) transcript levels demonstrated a robust 494-, 106-, and 29-fold increase, respectively. CEBPA, a leucine zipper family transcription factor, was reported to be expressed in differentiating lung epithelial AT2 cells, and its activity was linked with integrin signaling pathways [20]. The level of *Itga5*, *Itga6*, *Itgb1*, and *Itgb4* increase was 5- to 63-fold in SPCs during this 7-day period. In contrast, the levels of epithelial surfactant protein C (*Sftpc*) and secretoglobin 1A type 1 (*Scgb1a1*) transcripts decreased by 4- and 41-fold, respectively. By day 21 in culture, the myofibroblastic-like cells showed an increase in *Fn1*, *Col1a1*, and all studied integrins, ranging from 95 to more than 3,000-fold, compared with cells at day 0 (Table 1). Similarly, on SPC transition to a myofibroblast-like phenotype (comparing days 7 and 21), a significant increase in gene expression, ranging from 2.5- to 60-fold, prevailed for *Acta1*, *Col1a1*, *Fn1,* and all investigated integrins ($n \geq 4$; $p < .05$, for all by *F* test). *Cebpa* gene expression showed a significant eightfold decline in production ($p < .001$), and no differences in endothelial *Cd31* or epithelial *Sftpc* and *Scgb1a1* expression were observed between the cell types. To confirm that long-term SPC cultivation produces cells of a lung fibroblast lineage, we used qPCR and flow cytometry to determine the expression of predominant mesenchymal and integrin markers in both AIC-derived myofibroblasts and primary lung myofibroblast cultures. Of all the genes tested, which included *Acta1*, *Col1a1*, *Fn1*, *Itga5*, *Itga6*, *Itgb1*, and *Itgb4*, despite an average fourfold increase in *Col1a1* expression in SPC-derived myofibroblasts, no statistically significant differences in gene expression were observed between the cell types ($n \geq 4$; supplemental online Fig. 4). Using flow cytometry, we then compared the percentage of ACTA1 expressing cells between AIC-derived and lung-derived (primary) myofibroblastic cells. No significant difference was found, with 94.8% $\pm$ 3.6% and 98.7 $\pm$ 0.8% of AIC-derived and lung-derived myofibroblasts producing ACTA1, respectively (n = 4; Fig. 4A, 4B). Taken together, these data indicate that SPCs develop into cells of the myofibroblast lineage and that this process can now be studied in tissue-culture settings.

Table 1. Gene expression changes of pulmonary-derived stromal cell lineage derivatives

Gene/lineage	SPC	Myofibroblast
Acta1	0.8 ± 0.6	2.1 ± 1.4[a]
Cd31	3.4 ± 0.9	3.7 ± 2.0
Cebpa	28.7 ± 16.3	3.5 ± 1.8[b]
Col1a1	106.2 ± 58.5	1119.6 ± 746.8[b]
Fn1	494.2 ± 201.2	3327.1 ± 694.3[c]
Itga5	63.3 ± 38.7	319.5 ± 99.9[a]
Itga6	4.7 ± 1.6	94.7 ± 47.8[b]
Itgb1	5.8 ± 1.2	345.8 ± 149.6[b]
Itgb4	12.5 ± 7.6	226.3 ± 76.7[b]
Sftpc	0.2 ± 0.1	0.3 ± 0.2[a]
Scgb1a1	0.0 ± 0.0	0.0 ± 0.0[c]

Data are presented as $2^{-\Delta\Delta Ct}$ (mean ± SEM). Quantitative PCR demonstrating selected gene levels in SPCs and their resulting myofibroblasts ($n \geq 6$ for each gene). Threshold cycle (Ct) values were normalized to *Gapdh* expression and the original AIC population. Genes tested included α smooth muscle actin (*Acta1*); Cd31/Pecam 1 (*Cd31*); CCAAT/enhancer-binding protein α (*Cebpa*); collagen type I α 1 (*Col1a1*); fibronectin 1 (*Fn1*); integrin α 5 (*Itga5*); integrin α 6 (*Itga6*); integrin-β1 (*Itgb1*); integrin-β4 (*Itgb4*); surfactant protein-C (*Sftpc*); and secretoglobin, family 1A, member 1 (*Scgb1a1*). Production of extracellular matrix and integrin transcripts were significantly higher in differentiated myofibroblasts. Statistical significance between myofibroblasts and their SPC progenitors was determined using the *F* test.

[a] $p \leq .05$.
[b] $p \leq .001$.
[c] $p \leq .01$.
Abbreviations: PCR, polymerase chain reaction; SPCs, stromal progenitor cells.

Integrins and VLA5 Play an Important Role in Myofibroblast Cell Development

With a robust increase in transcription, we next investigated the ensuing changes in integrin protein expression that might occur during myofibroblast lineage development. We focused on ITGA5, ITGA6, ITGB1, and ITGB4 membrane surface expression, all reported to serve as progenitor cell markers. Flow cytometry analysis indicated that although the percentage of cells producing ITGB1 significantly increased ($p < .01$), the proportion of cells producing ITGA5 decreased with cell maturation ($n \geq 10$; data not shown). These results were intriguing, given an increase in the *Itga5* transcript (see previous section) and an average 56% increase in the ITGA5 protein signal, as determined by densitometric analysis of immunoblot assays (supplemental online Fig. 2; $n = 3$; $p = .04$), and a 3.4- and 5.9-fold increase in the percentage of ITGA5/ITGB1 (VLA5) and ITGA5/ITGB4 double-positive cells with maturation, respectively (data not shown; $p \leq .03$ for both; $n \geq 4$). Therefore, to test the reliability of the flow cytometry data, which could be affected by proteolytic degradation of integrin subtypes at the cell dissociation step (trypsin and dispase processing showed similar results), we resorted to immunofluorescence, which does not require proteolysis before analysis. As seen in Figure 4C, integrin expression was punctate, with more than 98.7% ± 1.4% and 99.7% ± 0.1% of the cells positive for ITGA5 and ITGB1 labeling, respectively ($n = 3$; quantified by two independent observers). As evidenced from the data, ITGA5 expression was generally found to overlap with ITGB1 (VLA5) and the cell nucleus (represented by DAPI staining), and ITGA6, produced in 85.7% ± 7.1% of AIC-derived myofibroblast cells, showed little overlap with ITGB1 or the nucleus. Consistent with an increase in the percentage of integrin expressing cells, myofibroblast cell differentiation also involves greater cell production of ITGA5 and ITGB1 and their heterodimerization to form VLA5.

Fibrogenic Derivation of Renal and Cardiac SPCs Recapitulates That of the Lung

Fibroblasts of the kidney and heart, similar to those of the lung, deposit connective tissue and, on hyperactivation, have been reported to trigger organ fibrosis. Therefore, to test whether we could direct renal and cardiac SPC differentiation into myofibroblastic cell types (in a fashion similar to that of the lung, shown in Fig. 1A), we performed separate cultures of autologous murine kidney and heart tissue. In these studies, similar to those of the pulmonary SPCs, organotypic kidney and heart SPCs differentiated into myofibroblasts, as determined by immunochemistry for COL1A1 and FN1 and the formation of β-actin stress fibers, all common to myofibroblastic cell types (Fig. 5; $n \geq 4$). These data suggest that SPCs can be found in multiple tissues and that these cells give rise to indigenous myofibroblastic cell types.

Pulmonary AIC-Derived Lineages Engraft in Immunocompetent Recipient Mouse Lungs

The AIC population of cells was previously reported to compose a subset of epithelial progenitor cell types [16]. Because we had established the presence of a subset of stromal cell progenitors with the inherent capability to attach, grow, and differentiate in culture, we next sought to determine the differentiation properties of these cells in an in vivo model. For these experiments, 1–2-week (expanded) allogeneic AICs from hemizygous β-galactosidase (β-gal; representative staining can be seen in supplemental online Fig. 5) or GFP reporter mice were instilled by tracheal incision into the airspaces of immunocompetent wild-type mouse lungs [19]. At several time points after transplantation, the recipient mice were sacrificed, with the lungs harvested and tested for cell retention and lineage by gene analysis and immunochemistry (Fig. 6A). Our data demonstrated β-gal$^+$ cell foci retention in the lungs of recipient mice for up to 2 months in vivo with no significant background staining observed (Fig. 6B, 6C). Moreover, at 2 months, the transplanted cells were found to connect with the adjacent alveolar walls (Fig. 6D; arrowhead), with donor tissue displaying alveolar type 2 epithelial, surfactant protein C (SFTPC), and stromal FN1 extracellular matrix protein production ($n \geq 4$; Fig. 6E). To validate cell colonization of the lung, we isolated GFP-reporter AICs and grafted them into recipient mouse left lungs. Representative images of control (contralateral) and GFP-instilled (ipsilateral) lungs after 2 months in vivo are shown in supplemental online Fig. 6. We subsequently quantified the maximal GFP fluorescent intensity in selected regions of the ipsilateral and contralateral lobes (Fig. 6F; $n \geq 10$ regions from four separate transplantation experiments). The GFP signal in the ipsilateral lobe of transplanted mice showed on average a statistically significant 4.5-fold increase compared with the background fluorescence of the contralateral lung ($p < .01$). Epithelial differentiation of implanted AICs was observed in transplanted lung sections by coimmunofluorescence of GFP, SFTPC,

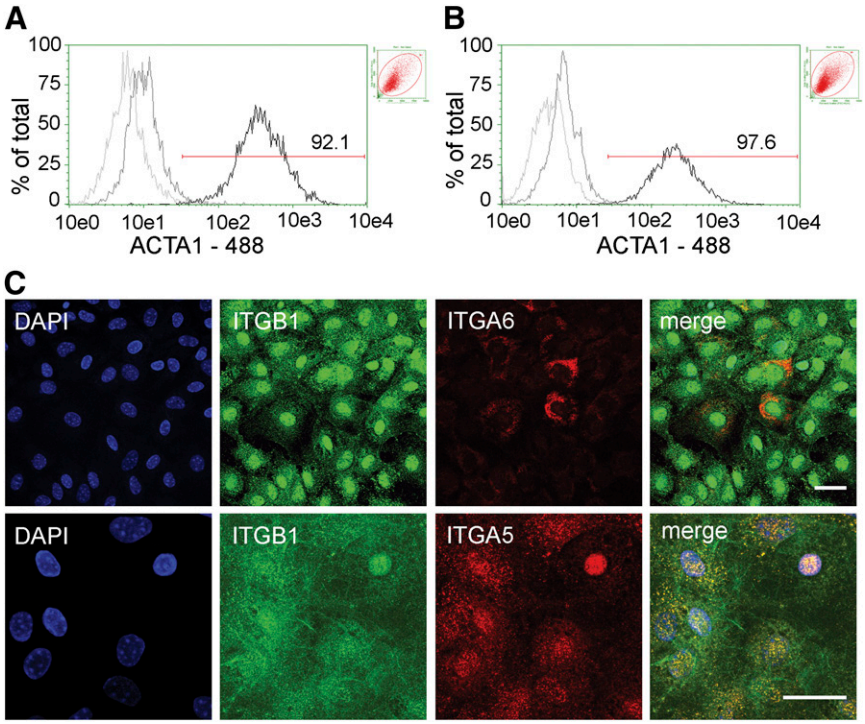

Figure 4. ACTA1 and very late antigen-5 (VLA5) production in stromal progenitor derived myofibroblasts. Fibroblasts were collected, permeabilized, and ACTA1 or VLA5 and VLA6 presence was tested. Representative flow cytometry histograms depicting percentage of ACTA1 protein expression in fibroblasts derived from anchorage-independent cells **(A)** and primary lung cultures **(B)**. Untreated (light gray), isotype (dark gray), and ACTA1-treated (black) cell populations are shown. Percentage of ACTA1-positive cells is also shown. Insets: Respective forward scatter vs. side scatter plots. **(C):** Cellular localization of ITGA5, ITGA6, and ITGB1 subunits in SPC-derived fibroblasts as seen by immunofluorescence. Top (from left to right): DAPI nuclear stain (blue), ITGB1 (green), ITGA6 (red), and Merge. Bottom (from left to right): DAPI nuclear stain (blue), ITGB1 (green), ITGA5 (red), and Merge. ITGA5 localization predominantly corresponds to that of ITGB1 to form VLA5 (yellow) focal adhesions in fibroblastic cells. Scale bars = 20 μm. Abbreviations: 488, Alexa Fluor 488; ACTA1, α smooth muscle actin type 1; DAPI, 4′6-diamidino-2-phenylindole; ITGA5, integrin α-5; ITGA6, integrin α-6; ITGB1, integrin β-1.

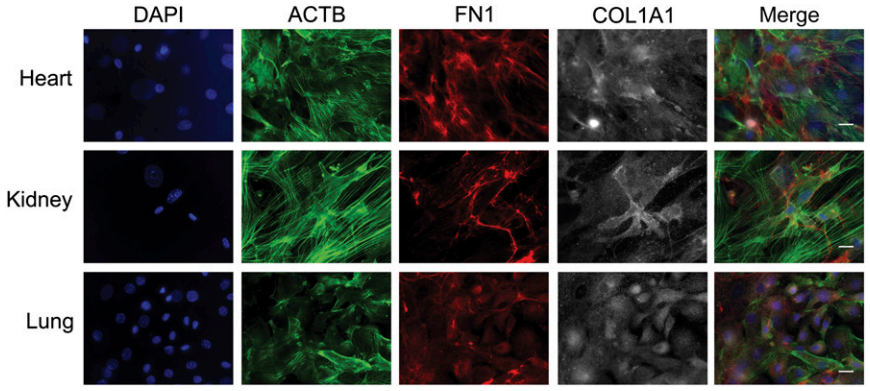

Figure 5. Organotypic progenitor cell differentiation into myofibroblasts. Autologous heart, kidney, and lung anchorage-independent cells were isolated from mice, differentiated toward the myofibroblastic lineage, and prepared for immunofluorescence ($n \geq 4$). Representative micrographs of heart (top), kidney (middle), and lung (bottom) are shown. Differentiated myofibroblasts at day 80 in culture were stained with DAPI (blue), the actin binding drug phalloidin (ACTB; green), and labeled for FN1 (red) and COL1A1 (gray) proteins. Scale bars = 20 μm. Abbreviations: ACTB, β-actin; COL1A1, collagen type 1 α 1; DAPI, 4′6-diamidino-2-phenylindole; FN1, fibronectin-1.

and SCGB1A1 (supplemental online Fig. 7). SCGB1A1 is a notable marker for secretory epithelial (and progenitor) cell types of the terminal bronchioles. To confirm cellular retention in the host, we isolated AICs from male mice and allografted them into female recipients. The lungs were harvested after 1 month, the tissue lysed, and DNA extracted. PCR primers specific for *Sry* and *Mecp2* gene sequences were used to determine the presence of Y and/or X chromosomes, respectively. As shown in Figure 6G, although the X-linked *Mecp2* gene was expressed in all mouse tissues examined, the *Sry* gene was predominantly identified in the lungs of the intratracheally engrafted females. In contrast, freshly prepared male pneumocyte isolates transplanted into a female were not retained in the host lung over the same period ($n = 4$; $p < .05$). These data indicate that

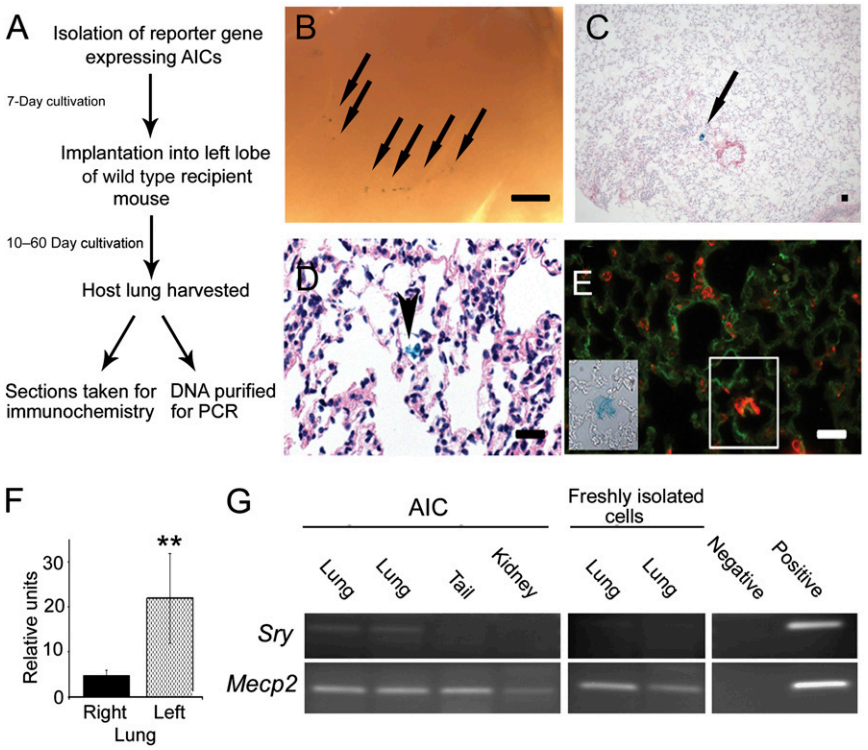

Figure 6. Progenitor cell incorporation in the intact lung. **(A):** Flowchart depicting experiments of pulmonary isolation, transplantation (1×10^6 cells), and donor cell identification in recipient mouse lungs. **(B):** Macroscopic view of a day-10 post-transplantation lung grafted with β-galactosidase (β-gal)-expressing AICs. Scale bar = 1 mm. Arrows depict regions rich in indigo-stained cells. **(C):** Low power, hematoxylin eosin-stained section of a day 30 (post-transplantation) recipient lung demonstrating β-gal-positive cells in the alveolus (arrow). **(D):** High power, hematoxylin eosin-stained recipient lung section illustrating grafted β-gal-labeled cells (arrow) with connective tissue characteristics, bridging adjacent alveolar tissues. Scale bar = 100 μm. **(E):** High power image of a transplanted mouse alveolus collected at day 60 after transplantation demonstrating a region of prosurfactant protein C (red) and fibronectin-1 (green) expression (white box) that corresponds with β-gal-positive donor cell expression (inset). Scale bar = 50 μm. **(F):** Histogram comparing the average fluorescent intensities of selected ipsilateral and contralateral lung regions of mice (day 30 after transplantation) grafted with green fluorescent protein reporter cells. Differences in signal intensities are statistically significant ($n = 4$; $p < .01$, Wilcoxon test). Finally, male donor AICs or freshly isolated lung cells were transplanted into recipient female mice. After 30 days, distinct organs were harvested, and DNA was amplified. **(G):** Chromosome Y-linked *Sry* sequences were detected in the lungs but not in the tail or kidney of transplanted female mice at day 30. The X-linked *Mecp2* gene, found in all cells, was used as a control. Implantation of freshly isolated cells (male, lung) did not show any retention in female recipients at the same time point. These differences are statistically significant ($n = 4$; $p < .05$). Negative and positive PCR controls represent no and male C57BL/6 DNA controls, respectively. Abbreviations: AIC, anchorage-independent cell; PCR, polymerase chain reaction.

cultivated AIC allografts differentiate into epithelial and fibroblastic cell types in recipient mice and that these lineages are maintained for a 2-month growth period.

Discussion

Environmental and physiological conditions can influence the genetic programs that drive stem/progenitor cell differentiation. We have demonstrated a method in which a mixed population of progenitor cells, from multiple tissues, can emulate an in vivo environment of compensatory growth. Accordingly, we have established the physiological and molecular properties that can now be used to define stages of cell differentiation, manifested by an attachment-mediated shift toward stromal cell and specification toward the myofibroblast lineage. These changes are accompanied by increased ECM component expression and VLA5 assembly. Finally, extending these findings, we have demonstrated that transplanted AICs can repopulate an immunocompetent host lung, contributing to both epithelial and fibroblastic cell lineages.

Our findings are consistent with the existence of a mixed anchorage independent progenitor cell population and extend previous findings that elucidated a key role for integrin subunit expression and their function in stem cell differentiation [21–23]. More importantly, these data support the existence of an early stromal cell, which lacks conventional markers and morphologies, that might be involved in lung, kidney, and heart pathologic entities and in cancer [24–26].

Developmental signals that influence progenitor cell decisions can result from stochastic intracellular programs or cues from the microenvironment [22, 27]. Because epithelial to mesenchymal transition does not seem to occur in vivo, the primary source of fibrotic cells seems to be the circulating fibrocyte/monocyte [28–30]. Accordingly, because SPCs originate from a free-floating population, we speculate that fibrocytes in vivo are the source of the SPCs in our model and that, collectively, these cells form an elaborate network of cooperative development required for healthy tissue/organ regeneration. Using this analogy, major changes to, or experimental removal of, one node from the network could increase the

instability of the remaining nodes and, in turn, trigger genetic rewiring and differentiation down an alternate path. Accordingly, removal of free-floating epithelial progenitors from the SPC culture might trigger these changes and initiate myofibroblastic cell development. Taken together, myofibroblast differentiation in vitro is governed by a two-step process: an initial protein-mediated attachment to the substrate, followed by gene-driven cell remodeling and hyperproliferation.

We speculate that the initial trigger of fibroblastic development in this model is a release from low density free-floating AICs, by a molecular breakdown of cell-cell interactions, and descent to the substrate (by gravity). Attachment to the surface through substrate binding (focal adhesive) integrins would subsequently promote cell reprogramming. To support this model, gravity was shown to induce changes on cell cytoskeletal and focal adhesion components and to specifically affect ITGB1 expression on human MCF7 cells [31]. We found that ITGB1 plays an important role in myofibroblastic development, which, together with ITGA5, forms VLA5. We also demonstrated that this prominent phenotype can be masked in cellular assays that require proteolytic steps for single cell dissociation, in particular, flow cytometry.

In the present study, we chose to investigate the cellular production of the ITGA5 and ITGA6 integrin subtypes, in addition to ITGB1 and ITGB4, because of reports that suggest their value in characterizing various progenitor and proliferating cell types. Our findings elaborate on the differences in ITGA5-, ITGB1-, and VLA5-expressing cells, with ITGB1 expression and VLA5 assembly increasing in differentiated myofibroblasts. Hence, it is plausible that integrin expression patterns might be better predictors of migrating stromal than quiescent progenitor cells. In an inside-out fashion, integrin conformation can be modified to promote ECM attachment, degradation, and internalization [32]. Production of COL1A1, found in mesenchymal cells of the neonate lung and myofibroblast progenitor cells, and FN1, the expression of which is significantly increased during development and wound healing, would assist in integrin-mediated cell motility [33–35]. In an outside-in fashion, ITGB1 activation could potentiate fibroblast differentiation through phospholipase A2 activation and arachidonic acid (AA) signaling [36]. AA metabolism was shown to stimulate the cellular adherence of alveolar macrophages to plastic, to be elevated in AT2 cells undergoing mesenchymal transformation, and to further enhance ITGB1 activity and FN1 expression [37–41]. Furthermore, in fibroblasts, AA pathway activation was demonstrated to induce cell remodeling and dispersal [36]. With applications to interstitial lung diseases and pulmonary fibrosis, understanding the fibroblast precursor and the molecular mechanisms active during cell attachment and differentiation remain important topics for future studies.

Cell delivery is a major challenge in the implementation of stem cell therapies. To date, studies that focused on the engraftment of stem cells and their primary cultured derivatives into the lungs of healthy immunocompetent mice have demonstrated modest or no retention [42–45]. Significantly, we established epithelial and fibroblast cell retention in the mouse lung for up to 2 months in vivo. At this point, the prevalence of multilineage donor cells that do not demonstrate mitotic activity in the recipient lung (data not shown), together with a lack of SPC reversal to a free-floating state (in culture), repudiates the concept of progenitor cell dedifferentiation. Thus, we have established that AIC attachment and viability in vivo conform to those observed in culture and that the final path of progenitor cell development is influenced by cell programming and microenvironmental pressures. In summary, our approaches revealed multiorgan SPC differentiation into myofibroblastic cell types and demonstrated that intratracheal cell engraftment is a practical route to provide structural and functional building blocks to the lung.

Our findings should be interpreted in the context of the study design. We report that a previously described mixed free-floating, $CD45^+/CD11b^+$ (macrophage), and epithelial stem cell population additionally harbors a stromal progenitor subset. SPCs can be selected by physiological anchoring properties rather than immunophenotype and can develop into functional MSC and fibroblastic cell lineages. Although it remains unclear whether the reported SPC is represented early in the AIC or develops as an adaptation to two-dimensional culture, one unique characteristic of this cell is rooted in its development. Specifically, during isolation, SPCs are not segregated from the rest of the tissue by enzymatic proteolysis and/or subjected to the possibility of antibody-mediated cell signaling. These treatments are necessary in many immunophenotyping assays and, as shown by us and others, can cause robust cellular artifacts [46].

On implantation of pulmonary AICs into the intact mouse lung, we observed high cellular resilience and retention for more than 2 months in vivo. Although we did not detect donor cell division, it is possible that mitosis did occur in vivo; however, our sample size was too small to identify it, because only 1% of SPCs displayed division in vitro. By extension, these data would give us a 1 in 100 chance to identify this process. In addition, because the recipient lungs were exposed to stress during the transplantation procedure, possibly leading to epithelial barrier damage, we must consider the notion that the implanted cells fused with endogenous cells or were endocytosed by residential phagocytes [47]. Nevertheless, although possible, these scenarios were unlikely, because both alveolar and peribronchial spaces of the lung were populated by donor cells, and the frequency of intratracheally instilled cell fusion was reported to be low [42]. Furthermore, multinucleated cells were not observed, and the half-life of the enhanced-GFP reporter protein in fibroblasts was reported to be on the order of hours and not of days [48]. Finally, we did not identify a robust immune response to the allografted cells in all sections tested. This is particularly encouraging, because tissue rejection is a common occurrence in human lung transplants. Taken together, these data indicate de novo gene expression of grafted cells in the lung for extended periods. Additional experiments to determine the fate of implanted cells in models of lung injury and of decellularized biological lung scaffolds are warranted.

In conclusion, we have demonstrated a subset of cells from multiple organs that, on attachment to a substratum, multipotentially beget cells of the stromal lineage. Through a program of differentiation, these cells increase ECM protein expression and enhance interactions and communications with their environment through VLA5. Understanding stromal cell differentiation can help expand our knowledge of myofibroblast activity in fibrosis and assist in cell-directed delivery to sites of organ degeneration.

Acknowledgments

This work was supported, in part, by the Henry and Bertha Kressel and Joseph Alexander Foundations and Yeshiva University start-up funds. We thank Drs. Vera DesMarais and Christina Polumbo from the Einstein Analytical Imaging Facility, the Ruth L. and David S. Gottesman Institute for Stem Cell Biology and Regenerative Medicine at the Albert Einstein College of Medicine, and, in particular, Drs. Simon Spivack and Eric Bouhassira for their helpful discussions.

Author Contributions

N.S. and M.W.: collection and/or assembly of data; Y.P.: conception and design, financial support, data analysis and interpretation, manuscript writing, final approval of manuscript.

Disclosure of Potential Conflicts of Interest

The authors indicate no potential conflicts of interest.

References

1 Keating A. Mesenchymal stromal cells: New directions. Cell Stem Cell 2012;10:709–716.

2 Johnson K, Zhu S, Tremblay MS et al. A stem cell-based approach to cartilage repair. Science 2012;336:717–721.

3 Paxson JA, Gruntman AM, Davis AM et al. Age dependence of lung mesenchymal stromal cell dynamics following pneumonectomy. Stem Cells Dev 2013;22:3214–3225.

4 Bernardo ME, Fibbe WE. Mesenchymal stromal cells: Sensors and switchers of inflammation. Cell Stem Cell 2013;13:392–402.

5 Alberts B, Johnson A, Lewis J et al. Molecular Biology of the Cell 2008;5th ed.New York, NYGarland Science.

6 Halfon S, Abramov N, Grinblat B et al. Markers distinguishing mesenchymal stem cells from fibroblasts are downregulated with passaging. Stem Cells Dev 2011;20:53–66.

7 Pierce RA, Griffin GL, Mudd MS et al. Expression of laminin alpha3, alpha4, and alpha5 chains by alveolar epithelial cells and fibroblasts. Am J Respir Cell Mol Biol 1998;19: 237–244.

8 White SR, Dorscheid DR, Rabe KF et al. Role of very late adhesion integrins in mediating repair of human airway epithelial cell monolayers after mechanical injury. Am J Respir Cell Mol Biol 1999;20:787–796.

9 Shen Q, Wang Y, Kokovay E et al. Adult SVZ stem cells lie in a vascular niche: A quantitative analysis of niche cell-cell interactions. Cell Stem Cell 2008;3:289–300.

10 Lakins JN, Chin AR, Weaver VM. Exploring the link between human embryonic stem cell organization and fate using tension-calibrated extracellular matrix functionalized polyacrylamide gels. Methods Mol Biol 2012;916: 317–350.

11 Rodin S, Domogatskaya A, Ström S et al. Long-term self-renewal of human pluripotent stem cells on human recombinant laminin-511. Nat Biotechnol 2010;28:611–615.

12 Couchman JR, Höök M, Rees DA et al. Adhesion, growth, and matrix production by fibroblasts on laminin substrates. J Cell Biol 1983;96: 177–183.

13 Robledo MM, Sanz-Rodriguez F, Hidalgo A et al. Differential use of very late antigen-4 and -5 integrins by hematopoietic precursors and myeloma cells to adhere to transforming growth factor-beta1-treated bone marrow stroma. J Biol Chem 1998;273:12056–12060.

14 Nystedt J, Anderson H, Tikkanen J et al. Cell surface structures influence lung clearance rate of systemically infused mesenchymal stromal cells. Stem Cells 2013;31:317–326.

15 Even-Ram S, Yamada KM. Cell migration in 3D matrix. Curr Opin Cell Biol 2005;17: 524–532.

16 Peter Y, Sen N, Levantini E et al. CD45/CD11b positive subsets of adult lung anchorage-independent cells harness epithelial stem cells in culture. J Tissue Eng Regen Med 2013;7:572–583.

17 Peter Y, Comellas A, Levantini E et al. Epidermal growth factor receptor and claudin-2 participate in A549 permeability and remodeling: Implications for non-small cell lung cancer tumor colonization. Mol Carcinog 2009;48: 488–497.

18 Sen N, Weprin S, Peter Y. Discrimination between lung homeostatic and injury-induced epithelial progenitor subsets by cell-density properties. Stem Cells Dev 2013;22: 2036–2046.

19 Peter Y. Tracheotomy: A method for transplantation of stem cells to the lung. J Vis Exp 2007;(2)163.

20 Bassères DS, Levantini E, Ji H et al. Respiratory failure due to differentiation arrest and expansion of alveolar cells following lung-specific loss of the transcription factor C/EBPalpha in mice. Mol Cell Biol 2006;26: 1109–1123.

21 Notta F, Doulatov S, Laurenti E et al. Isolation of single human hematopoietic stem cells capable of long-term multilineage engraftment. Science 2011;333:218–221.

22 McQualter JL, Yuen K, Williams B et al. Evidence of an epithelial stem/progenitor cell hierarchy in the adult mouse lung. Proc Natl Acad Sci USA 2010;107:1414–1419.

23 Laird DJ, von Andrian UH, Wagers AJ. Stem cell trafficking in tissue development, growth, and disease. Cell 2008;132:612–630.

24 Runswick SK, O'Hare MJ, Jones L et al. Desmosomal adhesion regulates epithelial morphogenesis and cell positioning. Nat Cell Biol 2001;3:823–830.

25 Green FH, Williams DJ, James A et al. Increased myoepithelial cells of bronchial submucosal glands in fatal asthma. Thorax 2010;65: 32–38.

26 Zhang Z, Lee JC, Lin L et al. Activation of the AXL kinase causes resistance to EGFR-targeted therapy in lung cancer. Nat Genet 2012;44:852–860.

27 Doupé DP, Alcolea MP, Roshan A et al. A single progenitor population switches behavior to maintain and repair esophageal epithelium. Science 2012;337:1091–1093.

28 Hashimoto N, Jin H, Liu T et al. Bone marrow-derived progenitor cells in pulmonary fibrosis. J Clin Invest 2004;113:243–252.

29 Mesure L, De Visscher G, Vranken I et al. Gene expression study of monocytes/macrophages during early foreign body reaction and identification of potential precursors of myofibroblasts. PLoS One 2010;5:e12949.

30 Rock JR, Barkauskas CE, Cronce MJ et al. Multiple stromal populations contribute to pulmonary fibrosis without evidence for epithelial to mesenchymal transition. Proc Natl Acad Sci USA 2011;108:E1475–E1483.

31 Li J, Zhang S, Chen J et al. Modeled microgravity causes changes in the cytoskeleton and focal adhesions, and decreases in migration in malignant human MCF-7 cells. Protoplasma 2009;238:23–33.

32 Simon DI, Ezratty AM, Francis SA et al. Fibrin(ogen) is internalized and degraded by activated human monocytoid cells via Mac-1 (CD11b/CD18): A nonplasmin fibrinolytic pathway. Blood 1993;82:2414–2422.

33 Popova AP, Bozyk PD, Goldsmith AM et al. Autocrine production of TGF-beta1 promotes myofibroblastic differentiation of neonatal lung mesenchymal stem cells. Am J Physiol Lung Cell Mol Physiol 2010;298: L735–L743.

34 Sinkin RA, LoMonaco MB, Finkelstein JN et al. Increased fibronectin mRNA in alveolar macrophages following in vivo hyperoxia. Am J Respir Cell Mol Biol 1992;7:548–555.

35 Limper AH, Roman J. Fibronectin: A versatile matrix protein with roles in thoracic development, repair and infection. Chest 1992; 101:1663–1673.

36 Auer KL, Jacobson BS. Beta 1 integrins signal lipid second messengers required during cell adhesion. Mol Biol Cell 1995;6:1305–1313.

37 Priante G, Musacchio E, Valvason C et al. EPA and DHA suppress AngII- and arachidonic acid-induced expression of profibrotic genes in human mesangial cells. J Nephrol 2009;22:137–143.

38 Wen Y, Gu J, Peng X et al. Overexpression of 12-lipoxygenase and cardiac fibroblast hypertrophy. Trends Cardiovasc Med 2003;13:129–136.

39 Palmantier R, George MD, Akiyama SK et al. Cis-polyunsaturated fatty acids stimulate beta1 integrin-mediated adhesion of human breast carcinoma cells to type IV collagen by activating protein kinases C-epsilon and -mu. Cancer Res 2001;61:2445–2452.

40 Lipchik RJ, Chauncey JB, Paine R et al. Arachidonate metabolism increases as rat alveolar type II cells differentiate in vitro. Am J Physiol 1990;259:L73–L80.

41 Kouzan S, Nolan RD, Fournier T et al. Stimulation of arachidonic acid metabolism by adherence of alveolar macrophages to a plastic substrate: Modulation by fetal bovine serum. Am Rev Respir Dis 1988;137:38–43.

42 Spees JL, Whitney MJ, Sullivan DE et al. Bone marrow progenitor cells contribute to repair and remodeling of the lung and heart in a rat model of progressive pulmonary hypertension. FASEB J 2008;22:1226–1236.

43 Leblond AL, Naud P, Forest V et al. Developing cell therapy techniques for respiratory disease: Intratracheal delivery of genetically engineered stem cells in a murine model of airway injury. Hum Gene Ther 2009;20:1329–1343.

44 Banerjee ER, Laflamme MA, Papayannopoulou T et al. Human embryonic stem cells differentiated to lung lineage-specific cells ameliorate pulmonary fibrosis in a xenograft transplant mouse model. PLoS One 2012;7: e33165.

45 Rojas M, Xu J, Woods CR et al. Bone marrow-derived mesenchymal stem cells in repair of the injured lung. Am J Respir Cell Mol Biol 2005;33:145–152.

46 Raiser DM, Kim CF. Commentary: Sca-1 and cells of the lung: A matter of different sorts. STEM CELLS 2009;27:606–611.

47 Herzog EL, Van Arnam J, Hu B et al. Threshold of lung injury required for the appearance of marrow-derived lung epithelia. STEM CELLS 2006;24:1986–1992.

48 Halter M, Tona A, Bhadriraju K et al. Automated live cell imaging of green fluorescent protein degradation in individual fibroblasts. Cytometry A 2007;71:827–834.

See www.StemCellsTM.com for supporting information available online.

